TRIBOLOGIA - Finnish Journal of Tribology 1-2 vol 39/2022

https://doi.org/10.30678/fjt.109837

SUOMEN TRIBOLOGIAYHDISTYS RY
THE FINNISH SOCIETY FOR TRIBOLOGY
www.tribologysociety.fi
https://journal.fi/tribologia

Wet Sliding Wear Behavior of EN31 Rolling Contact Bearings for Screw Compressor Application with Statistical Analysis

S.H. Gawande, Ketan Raykar
Department of Mechanical Engineering, M.E.S. College Of Engineering Pune, Maharashtra, S. P. Pune University, India
Corresponding author: S.H. Gawande (shgawande@gmail.com)

ABSTRACT

The aim of this work is to estimate the wear rate of EN31 material & obtain the line of best fit using statistical analysis of wear. In industrial screw compressors, EN31 is used as a material of construction for cylindrical roller bearings. The wet sliding phenomenon between the outer surface of the inner race of the rolling contact bearing & the outer surface of the cylindrical roller is simulated using pin-on-disk tribometer. Measurement of wear, friction force & friction coefficient is carried out by rubbing different cylinders of hardened EN31 against hardened EN31 disk of the pin-on-disk tribometer. Total 25 tests each of 10 minutes time duration are performed to estimate wear with variable loads in the range of 20 N to 100 N and speed in the range of 692 RPM to 1246 RPM. From experimental investigation using pin-on-disk tribometer & statistical analysis using MINITAB© commercial software, it is observed that the material wear rate of EN31 increases with the increase in load as well as increase in speed. From pin-on-disk experimentation & statistical analysis it is concluded that the load factor has higher effect on wear than the speed factor. It was observed that the wear increases with the load as well as with the speed.

Keywords: Screw compressor, Pin-on-disk tribometer, Wear rate, Friction coefficient, Statistical analysis, MINITAB®

1. INTRODUCTION

The objective of this research work is to study the tribological behavior of the bearing steels used for construction of cylindrical roller bearings which form an important part of the industrial screw compressor system. Research in tribology is important for the reduction of abrasive wear & friction forces in any two mating machine components in relative motion. EN31 is the widely used material for construction of inner & outer races of rolling contact bearings and also the cylindrical rollers. During operation, there is a relative motion between the outer surface of the rotating inner race & the outer surface of the cylindrical rollers which generates friction at the interface & also results in abrasive wear of both the mating components. The aim of tribological investigations of any mechanical system is minimization of friction forces & abrasive wear by application of a proper lubricant between the two surfaces in contact. This section summarizes the research work carried out by various researchers in the field of cylindrical roller bearings to study the tribological behavior of the system in order to minimize the resulting friction & wear.

Harris, et al. [1] carried out research in rolling bearing technology and studied kinematics, contact mechanics & tribological aspects of the rolling bearing technology. They described in detail the kinematics of cylindrical roller bearings & derived the mathematical expressions for angular & linear velocities of the same. Beswick, et al. [2] worked on various steel materials used for construction of bearings and discussed the manufacturing technology along with load-speed-lubrication aspects in the field of bearing technology. Bhushan [3] did fundamental research in the field of tribology to study experimentally the mechanisms of adhesive wear & abrasive wear for quantitative determination of material loss during the process of wear. Bhandari [4] explained the design of rolling contact bearings taking into consideration the industrial requirements along with selection from the vendor catalogues. Guillermo, et al. [5] carried out research on rolling bearing technology for refrigerant compressors and studied design of various types of refrigerant compressors and the influence of various lubricants on the tribological issues of rolling contact bearings. Li, et al. [6] evaluated cyclic contact stresses in cylindrical roller bearings using explicit finite element analysis and simulated fatigue crack initiation, crack growth & spalling. Liu, et al. [7] established a new method for modeling effects of natural defects on roller bearings and proposed a contact model taking into consideration the geometric features of the natural defects. Panda, et al. [8] maximized fatigue life of rolling contact bearing using Particle Swarm Optimization algorithm, whereas, Feldermann, et al. [9] used computational fluid dynamics to determine hydraulic losses in radial load cylindrical roller bearings. Denni, et al. [10] developed a novel multi-body dynamics model for simulation of rolling contact bearing mechanism in planetary applications. Laithy, et al. [11] investigated the effect of operating conditions such as pressure,

temperature & running time on rolling contact fatigue of bearings. Zhang, et al. [12] solved finite-length sliding contact problem using semi-analytical methods as Conjugate Gradient Method (CGM) and Fast Fourier Transform (FFT).

Guo, et al. [13] developed models to estimate cage speed and roller speed of cylindrical roller bearings considering the roller centrifugal forces, friction forces at the contact region, contact elasticity between the roller & the raceway & hydrodynamic lubrication. Ahmer, et al. [14] used pin-on-disk tribometer to measure friction coefficient & wear rate of aluminum metal at room temperature. Stratmann, et al. [15] evaluated growth of tribofilm in case of cylindrical roller thrust bearings operated in boundary lubrication regime. El-Thalji, et al. [16] worked on dynamic modeling of wear evolution considering tribological & topographical changes. They used multiple force diagrams to simulate the dynamic input. Takabi, et al. [17] studied dynamic behavior of radially-loaded roller bearings operating at low as well as high speeds considering different values of surface roughness. Eyre [18] explained industrial significance of different types of wear such as abrasive wear, adhesive wear, erosion, corrosion & fretting of various metals. Zhang, et al. [19] carried out mathematical analysis of friction mechanisms in sliding-rolling contacts in presence of elasto-hydrodynamic lubrication considering asperity interaction friction induced due to solid-to-solid ploughing & boundary film friction. This development was found to be a cost-effective method of estimation of friction coefficient in mixed elasto-hydrodynamic lubrication.

Gawande et al. [20] simulated the phenomenon of sliding gear tooth in planetary gear train application of CNC bending machine using pin-on-disk apparatus with 5 minutes duration tests for 50 N & 100 N loads at 350 rpm disk speed to study the variation of wear, friction force & friction coefficient with time. Dhanvij et al. [21] carried out tribological investigations on EN24 material for evaluation of friction coefficient, friction force & wear rate by sliding it against EN31 disk having 60 HRC hardness. Nicholas, et al. [22] used novel ultrasonic reflectometry techniques for measurement of roller loads in high-speed wind turbine gearbox. They bonded piezoelectric transducers on the outer raceway of the bearing. From the reflected pulses, bearing load was determined. Cavacece, et al. [23] worked on life evolution of rolling contact bearings subjected to high local contact pressures & low oscillatory speeds. Paulson et al. [24] worked on development of elastic-plastic finite element model for quantification of rolling contact fatigue of bearings made of case carburized steel. It was found that the ratio of the total rolling contact fatigue life of refurbished bearing to that of non-refurbished bearing was more for through hardened bearings as compared to the carburized bearings. Salguero, et al. [25] envisaged tribological issues during dry machining of Aluminum-Copper alloys along with Scanning Electron Microscopy (SEM) & Energy Dispersion Spectroscopy (EDS) analysis to study surface morphology of the material before & after wear.

Krishnaiah, et al. [26] presented industrial application of design of experiment & analysis of data and provided solution to various industrial problems using various techniques such as Taguchi design & analysis, statistical analysis including multiple regression analysis & randomized block design. Mathews [27] worked on design of experiments using MINITAB software. He focused on software approach for solving industrial problems using design of experiments & inferential statistics. Taguchi, et al. [28] worked on quality engineering issues in robust engineering technology used in industry. They focused on industrial application of design of experiments, Taguchi design, orthogonal arrays & signal-to-noise ratio. NSK Bearing Catalogues [29-33] are the vendor catalogues which give detailed information about design dimensions & selection of cylindrical rolling contact bearings used in screw compressors. These catalogues are very important from research point of view to know the existing technology in the field of rolling contact bearings. It also helps the researcher to know the scope of research in a particular rolling contact bearing manufactured by a particular vendor.

2. MATHEMATICAL MODELING

2.1 Cylindrical Roller Bearings in Screw Compressors

Cylindrical roller bearings (Fig.1) are widely used in screw compressors in the industry. Screw compressors are used in the industry for compressing process gases & refrigerant gases from suction pressures in the range of 0.01 MPa to discharge pressures in the range of 5 MPa. The suction volume flow rate for the gases flowing in screw compressors ranges from 200 m^3/h to 100000 m^3/h. The pressure ratio values used depend on the type of the gas which is compressed. The pressure ratios are in the range of 1.3 to 6. The compression can be carried out in single-stage or multi-stage arrangements. In screw compressors, the bearing loads are generated by gas pressure acting on the spiral rollers. Also, in the process of transmission of torque from one rotor to the other, rotor forces are generated which are transmitted to the bearings. Also, the screw compressors have input gears & timing gears. The radial and tangential forces acting on the gears are transmitted to the bearings. During startup of the screw compressor, loads are generated due to inertia of the spiral rotors. These forces are also transmitted to the bearings. Hence, there is a need to properly design the bearings of the screw compressor considering the criticality of loads & also the space constraints. In screw compressors, a proper combination of cylindrical roller bearings & angular contact bearings is used. The bearings are arranged such that the radial loads are taken only by the cylindrical roller bearings & the axial loads are carried only by the angular contact ball bearings. A correct radial clearance is maintained between the bearing outer raceway and its housing. Due to this radial clearance, the angular contact bearing cannot carry any radial load. Also, the cylindrical roller bearing can carry a very small amount of axial load if subjected to axial loading.

Fig.1 shows a cylindrical roller bearing used in screw compressors. A low-pressure process gas or refrigerant gas enters the screw compressor through its suction nozzle. It gets compressed by the spiral rollers which rotate continuously at high speeds. The compressed gas discharges through the outlet nozzle of the screw compressor.

2.2 Selection of Roller Bearing

In order to decide the dimensions (Table 1) of the cylindrical roller bearing, vendor catalog data of NSK Bearings as shown in the Fig. 2 & Fig. 3 is referred.

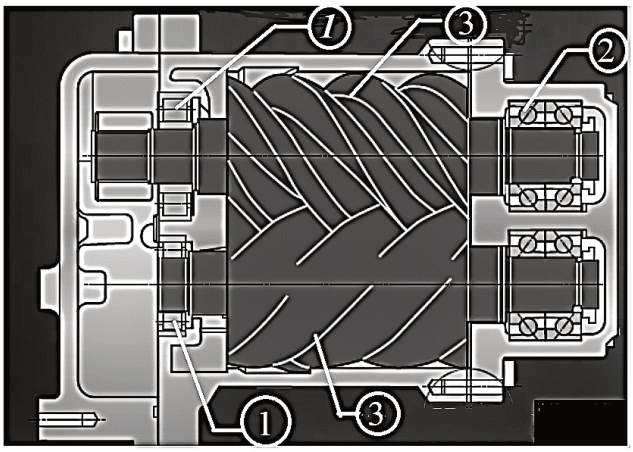

Fig. 1 Cylindrical roller bearings in screw compressors (1. Cylindrical roller bearing, 2. Ball bearing, 3. Spiral roller)

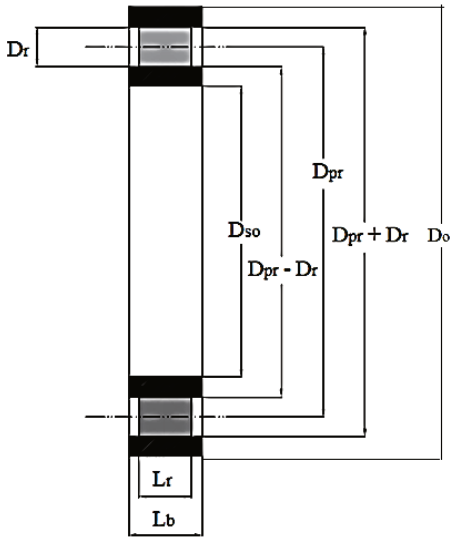

Fig. 2 Roller Bearing Dimensional Parameters

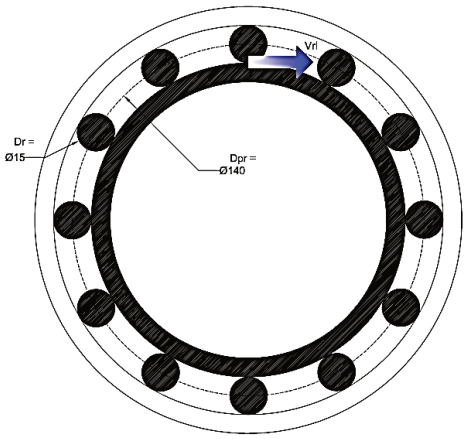

Fig. 3 Roller Bearing Dimension

2.3 Determination of Dynamic Load Carrying Capacity of the Bearing

The dynamic load carrying capacity of a cylindrical roller bearing is the amount of radial load the bearing can carry for a minimum life of one million revolutions. The life of a cylindrical roller bearing is the number of revolutions the bearing will complete just before the first occurrence of a fatigue crack in any of the cylindrical roller or in inner or outer races of the bearing. While calculating the dynamic load carrying capacity of a bearing, it is assumed that the inner race of the bearing is rotating & the outer race is stationery or fixed. The actual dynamic load carrying capacity of the bearing based on the empirical equation mentioned in the NSK bearing vendor catalog is estimated & then compared with the maximum dynamic loading capacity of the bearing mentioned in the same NSK bearing vendor catalog.

$$C_{Dyn} = c_{rf} c_{coeff} (n_{row} L_{eff} \cos\gamma)^{7/9} n_{roller}^{3/4} D_r^{29/27} \quad (1)$$

where, c_{rf} = 1.1, c_{coeff} = 86.4, n_{row} = 1, L_{eff} = 20 mm, γ = 0^0, n_{roller} = 12, D_r = 15 mm

Substituting this data in the Eq. (1),

C_{Dyn} = 115455 N

From NSK bearing vendor catalog, C_{Dyn} = 335000 N

∵ 115455 N < 335000 N, the design of the roller bearing & the cylindrical rollers is safe from dynamic loading capacity point of view.

The bearing life in million revolutions is given by the Eq. 2.

$$L_{10} = \frac{60 N_i L_{10h}}{10^6} \quad (2)$$

The screw compressors used for process gases & refrigerant gases operate at high rotational speeds. The maximum speed of the shaft coupled to the inner race as 3500 RPM is considered. Also, the bearings which are used in machinery for industrial applications require continuous operation of 24 hours per day. In case of pumps & compressors such as screw compressors used for process gas & refrigerant gas compression, the machines run for around 50000 hours.

Hence, N_i = 3500 RPM, L_{10h} = 50000 hours

∴ Substituting the above values in Eq.2, we get,

$$L_{10} = \frac{60 N_i L_{10h}}{10^6} = \frac{60 \times 3500 \times 50000}{10^6} = 10500$$

million revolutions.

Also, the radial load P_T acting on the rolling contact bearing is given by Eq.3.

$$P_T = \frac{C_{Dyn}}{(L_{10})^{0.3}} \quad (3)$$

∴ Substituting the values we get,

$$P_T = \frac{C_{Dyn}}{(L_{10})^{0.3}} = \frac{115455}{(10500)^{0.3}} = 7179 \text{ N}$$

Hence, 7179 N is the maximum load that the bearing can carry in the radial direction.

Table 1 Selection of roller bearing

Bearing Number (NSK Bearing Catalog)	Boundary Dimensions (NSK Bearing Catalog)			Basic Load Rating (NSK Bearing Catalog)		Estimated dimensions		
	D_{so}	D_o	L_b	C_{Dyn}	C_{St}	D_{pr}	D_r	L_r
	(mm)			(N)		(mm)		
NU (NJ) 2220 ET 7	100	180	46	335000	445000	140	15	20

2.4 Determination of Loads in Weight Pan for Pin-on-Disk Tribometer

Based on dynamic load carrying capacity of the bearing, the maximum radial load required to be carried by the cylindrical roller bearing is limited to 7179 N. This load will be shared by 12 cylindrical rollers.

P_T = Maximum Normal Load that can be carried by the bearing based on its dynamic load carrying capacity.

n_{roller} = Number of cylindrical rollers per row.

∴ Maximum load that can be carried by each cylindrical roller is:

$$\therefore P = \frac{4.36P_T}{n_{roller}} = \frac{7179}{12} = 2608.37 \text{ N} \quad (4)$$

Hence, the maximum normal static load that a cylindrical roller can carry is 2608.37 N.

This indicates that one can apply maximum 2608.37 N normal load on the roller while conducting simulation on pin-on-disk machine considering static & dynamic loading capacity of the bearing. Considering the limitations of the pin-on-disk machine, one can apply maximum load up to 20kg. hence it was decided to select loads as 20 N, 40 N, 60 N, 80 N &100 N. These loads lie within the limiting value of 2608.37 N.

2.5 Determination of Disk Speeds for Pin-on-Disk Experimentation

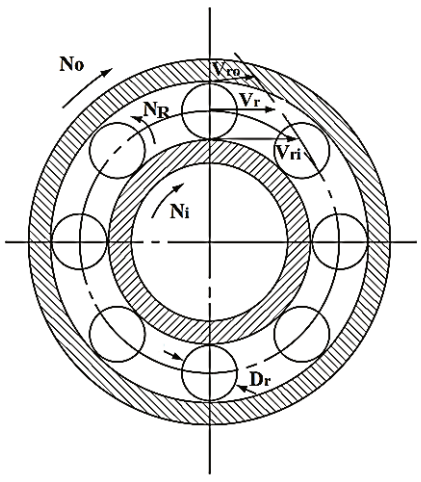

Fig. 4 Determination of disk speeds

The linear speeds of the inner & outer races of the bearing at the point of contact with the roller can be expressed by Eq. (5) and Eq. (6).

$$V_i = \frac{1}{2}\omega_i(D_{pr} - D_r) = \frac{1}{2} \times \frac{2\pi N_i}{60}(D_{pr} - D_r) = \frac{\pi N_i}{60}(D_{pr} - D_r) \quad (5)$$

$$V_o = \frac{1}{2}\omega_o(D_{pr} + D_r) = \frac{1}{2} \times \frac{2\pi N_o}{60}(D_{pr} + D_r) = \frac{\pi N_o}{60}(D_{pr} + D_r) \quad (6)$$

Considering there is no slip at the point of contact of the periphery of the roller & inner & outer races of the bearing (Fig.4). Therefore, the velocity of the cage & the rolling element is same & can be expressed as the mean value of the linear velocities of the inner & outer cages at the point of contact with the roller.

$$\therefore V_r = \frac{V_i + Vo}{2} = \frac{\pi}{120}\left[N_i(D_{pr} - D_r) + N_o(D_{pr} + D_r)\right] \quad (7)$$

Therefore, the rotational speed of the rollers & the cages about the axis of the shaft can be expressed as:

$$N_r = \frac{60V_r}{\pi D_{pr}} = \frac{1}{2}\left[Ni\left(1 - \frac{Dr}{Dpr}\right) + N_o\left(1 + \frac{D_r}{D_{pr}}\right)\right] \quad (8)$$

The rotational speed of the roller relative to the inner race can be expressed as:

$$N_{ri} = N_r - N_i = \frac{1}{2}\left[Ni\left(1 - \frac{D_r}{D_{pr}}\right) + No\left(1 + \frac{D_r}{D_{pr}}\right)\right] - N_i$$

$$\therefore N_{ri} = \frac{1}{2}\left(N_o - N_i\right)\left(1 + \frac{D_r}{D_{pr}}\right) \quad (9)$$

The linear speed of the roller relative to the inner race at the point of contact can be expressed as,

$$V_{ri} = \frac{1}{2}\omega_{ri}\left(D_{pr} - D_r\right)$$

$$\therefore V_{ri} = \frac{1}{2}\left(\frac{2\pi N_{ri}}{60}\right)\left(D_{pr} - D_r\right)$$

Substituting N_{ri} from Eq. (9)

$$\therefore V_{ri} = \frac{\pi}{60}\left(D_{pr} - D_r\right) \times \frac{1}{2}\left(N_o - N_i\right)\left(1 + \frac{D_r}{D_{pr}}\right)$$

$$\therefore V_{ri} = \frac{\pi}{120}\left(D_{pr} - D_r\right)\left(N_o - N_i\right)\left(1 + \frac{D_r}{D_{pr}}\right) \quad (10)$$

Now equating the linear speed of the roller relative to the inner race at the point of contact with the linear speed of the cylindrical test specimen relative to the rotating disk (Fig.5) of the pin-on-disk machine at the point of contact.

$$V_{ri} = V_t \quad (11)$$

$$\therefore \frac{\pi}{120}\left(D_{pr} - D_r\right)\left(N_o - N_i\right)\left(\frac{D_r}{D_{pr}} + 1\right) = \frac{1}{2}\omega_d D_t \quad (12)$$

Now, $$\omega_d = \frac{2\pi N_d}{60} \quad (13)$$

$$\therefore \frac{\pi}{120}\left(D_{pr} - D_r\right)\left(N_o - N_i\right)\left(\frac{D_r}{D_{pr}} + 1\right) = \frac{1}{2} \times \frac{2\pi N_d}{60} \times D_t$$

$$\therefore N_d = \frac{\left(N_o - N_i\right)}{2D_t}\left(D_{pr} - D_r\right)\left(\frac{D_r}{D_{pr}} + 1\right) \quad (14)$$

Hence selecting inner race rotating speeds as 1000 RPM, 1200 RPM, 1400 RPM, 1600 RPM & 1800 RPM and consider outer race to be stationary as it is fixed inside the screw compressor. From Eq. (14), the speed of rotation of the disk (N_d) of the pin-on-disk machine is calculated. Hence, the estimated rotational speeds of the disk corresponding to the inner race rotating speeds from Eq. (14) are 692 RPM, 830 RPM, 969 RPM, 1107 RPM & 1246 RPM respectively.

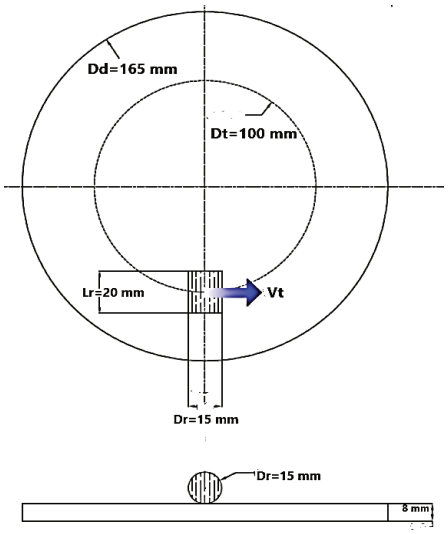

Fig. 5 Rotating disk

3. PROCESSING

3.1 Test Scheme

We adopted "Standard Test Method for Wear Testing with a Pin-on-Disk Apparatus" as mentioned in ASTM G99-95a (Reapproved 2000).

3.2 Chemical Composition & Mechanical Properties

EN31 is a commonly used metal in the manufacture of cylindrical rollers & races of antifriction bearings. The purchased EN31 material was tested in a laboratory to determine its chemical composition & mechanical properties (Table 2).

3.3 Sample Preparation

25 number of EN31 specimens were manufactured for experimental testing on pin-on-disk machine. The sample size is (15 mm Dia.) x (20 mm length). The specimens were prepared from the raw material by mechanical processes namely machining & heat treatment. The hardness of the specimens at various stages of manufacturing was tested in metallurgical testing laboratory & the values are as presented in Table 3. The EN31 specimens are through hardened. The material of the disc is EN31 & its hardness is 60 HRC.

3.4 Lubricant Selection

Lubricant ISO VG32 was selected based on the lubricant selection chart given in NSK bearing chart.

4. EXPERIMENTATION

Experimentation was performed on pin-on-disk machine to simulate the phenomenon of rolling & sliding contact between the outer surface of inner race of a roller bearing and the cylindrical roller. The hardened EN31 disk of the machine represents the inner race of the bearing & the test specimen held in the fixture which slides against the rotating disk represents the cylindrical roller. As shown in Fig.6 (a), the main components of the pin-on-disk machine are the rotating disk, friction sensor, wear sensor and linear variable differential transformer (LVDT). The wear, friction force & friction coefficient data generated during experimentation is saved on

(a)

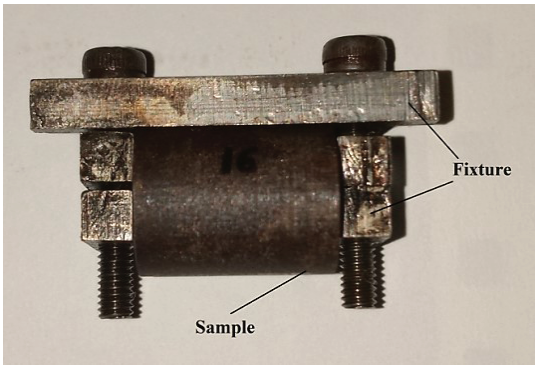

(b)

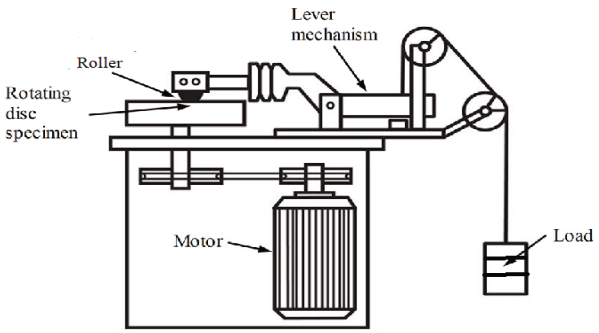

Fig. 6 (a) Experimental setup **(b)** Fixture for holding test specimens **(c)** Schematic of tribological test configuration

the computer hard disk with the help of WINDUCOM-10 software interface.Fig.6 (b) shows the fixture for holding the test specimens in position. The hardened EN31 disk of the machine rotates at the speeds set by the user. The stationary test specimen is allowed to slide against the rotating disk to simulate the rolling & sliding contact phenomenon which actually takes place during the operation of industrial cylindrical roller bearings. The loads acting on the test specimen are adjusted by placing suitable weights in the load pan of the machine. Total 25 tests each of 10 minutes duration were carried out on the pin-on-disk machine. The different combinations of disk speeds and loads in the weight pan are obtained in the form of an orthogonal array using Taguchi design as shown in Table 4.

5. RESULTS & DISCUSSION

5.1 Wear Pattern

During pin-on-disk experimentation, the EN31 steel test specimens experience rolling & sliding motion relative to the rotating disk on the pin-on-disk tribometer. Due to the friction force generated at the interface between the test specimen & the rotating disk, the test specimens get worn out & a specific wear pattern is observed on the peripheral surface of the test specimens.

Table 2 Chemical composition & Mechanical Properties of EN31 material

Elements	EN 31 (Reference)	EN 31 (Observed)
Carbon (C)%	0.90-1.20	0.980
Manganese (Mn)%	0.30-0.75	0.314
Silicon (Si)%	0.10-0.35	0.173
Sulphur (S)%	0.05	0.021
Phosphorus (P)%	0.05	0.014
Chromium (Cr)%	1.00-1.60	1.386
Nickel (Ni)%	------	0.032
Molybdenum (Mo)%	------	0.004
Aluminum (Al)%	------	0.012
Magnesium (Mg)%	------	0.003
Niobium (Nb)%	------	------
Lead (Pb)%	------	------
Tungsten (W)%	------	------
Titanium (Ti)%	------	------
Vanadium (V)%	------	------
Copper (Cu)%	------	0.006
Cobalt (Co)%	------	0.003
Ferrous (Fe)%	------	97.061

Material	EN31
Young's Modulus (N/mm^2)	200000
Poisson's Ratio	0.3
Hardness (HRC)	62 to 66
Melting Point (°C)	1424
Material Density (kg/m^3)	7810

Table 3 Hardness of EN31 Test specimens

Test No.	Sample	Testing Condition	Rockwell Hardness (HRC)	Brinell Hardness (BHN)
1		Before Machining	16 to 17	212 to 215
2		After Machining	12	193 to 195
3		After Heat Treatment	59 to 60	634 to 654

The wear pattern of the samples 1 to 25 used in the experiment number 1 is shown in the Fig. 7. The amount of material removed from a sample due to wear is proportional to the width of the white band appearing on its periphery. From Table 4, it can be seen that at a disk speed of 692 RPM, the amount of material removed increases from 17.410 µm to 118.610 µm as the load varied from 20 N to 100 N. At a disk speed of 830 RPM, the amount of material removed increases from 49.130 µm to 122.650 µm as the load is varied from 20 N to 100 N. At a disk speed of 969 RPM, the amount of material removed increases from 88.200 µm to 118.530 µm as the load is varied from 20 N to 100 N. At a disk speed of 1107 RPM, the amount of material removed increases from 111.700 µm to 144.870 µm as the load is varied from 20 N to 100 N. At a disk speed of 1246 RPM, the amount of material removed increases from 177.060 µm to 196.080 µm as the load is varied from 20 N to 100 N.

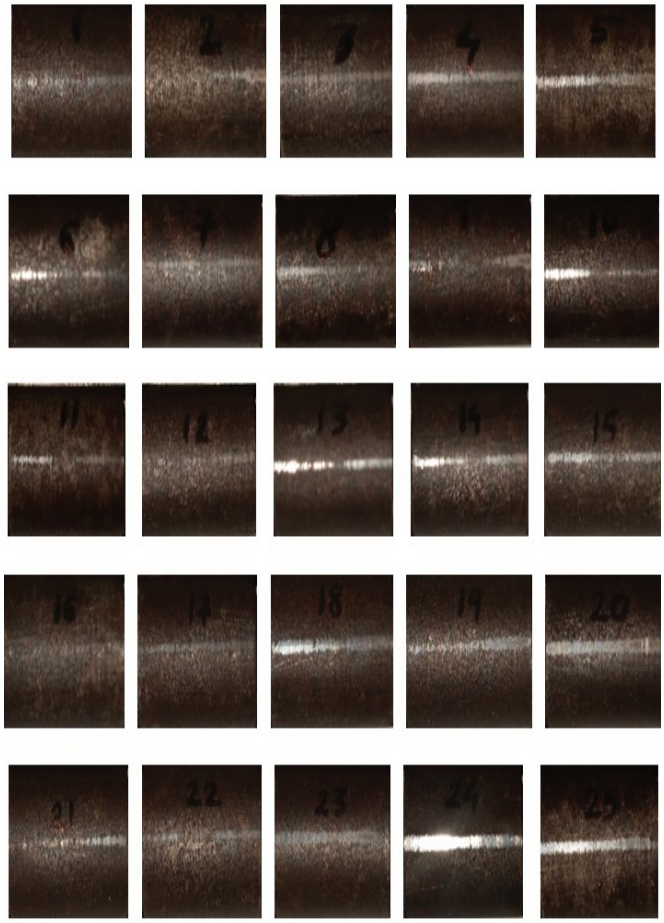

Fig. 7 Wear pattern of the worn-out test specimens

5.2 Representation of Measured Wear, Friction Force, Friction Coefficient

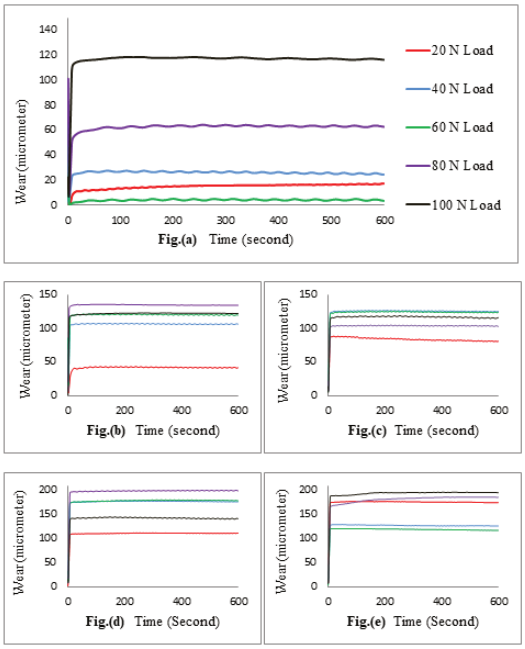

Fig. 8 Variation of wear with time

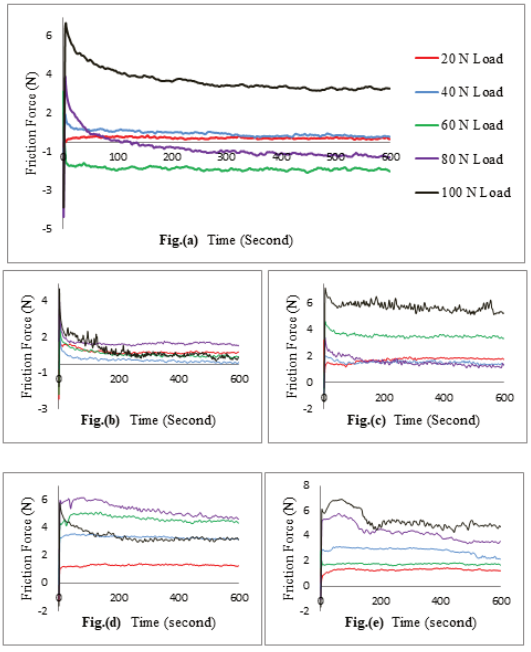

Fig. 9 Variation of friction force with time

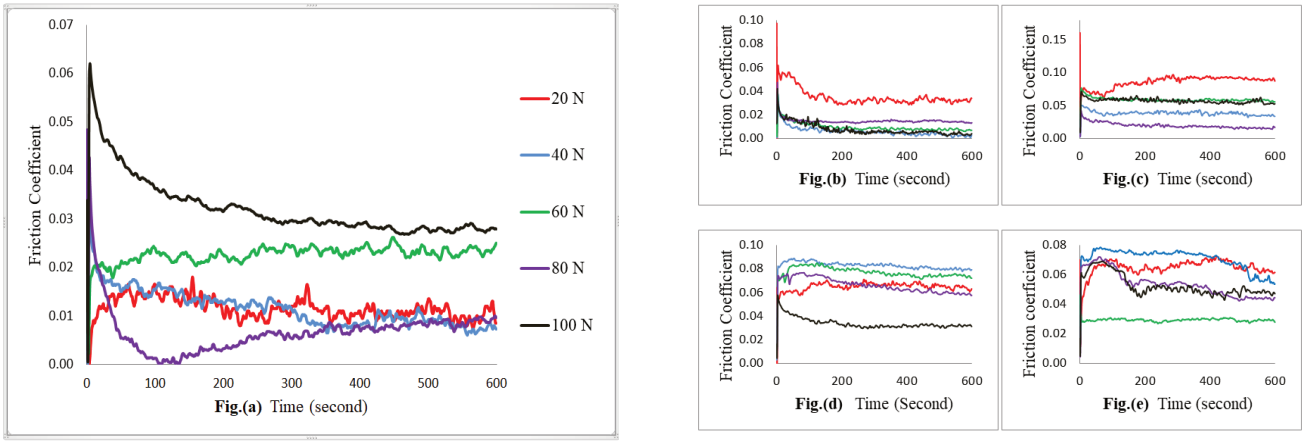

Fig. 10 Variation of friction coefficient with time

Figs.8-10 show the graphical representation of the measured data obtained from pin-on-disk experimentation.

These plots show the variation of wear (µm) with time (sec.), friction force (n) with time (sec.) and friction coefficient with time (sec.) respectively. The Figs. 8-10 (a), (b), (c), (d) and (e) represent the disk speeds of 692 rpm, 830 rpm, 969 rpm, 1107 rpm & 1246 rpm respectively. The red, blue, green, violet & black lines indicate the load magnitudes of 20 N, 40 N, 60 N, 80 N & 100 N respectively. Total 25 tests were carried out on 25 different EN31 test specimens for 10-minute duration each. The different combinations of speed & load as obtained by Taguchi design are shown in the Table 5 in the form of an orthogonal array.

From Fig. 8 (a-e) it is observed that initially the wear rises to a maximum value in a very short time interval & then remains steady for the remaining test duration. From Fig.9 (a-e) it is seen that initially the friction force rises to a maximum value, falls & then oscillates about a mean value for the remaining test duration. It can also be observed that the friction force changes from positive to negative or vice-versa for some tests. From Fig. 10 (a-e) it is observed that the friction coefficient initially rises to a maximum value in a very short time interval, oscillates & decreases to a minimum value in the remaining test duration.

5.3 Statistical Analysis of Experimental Results

- S/N Ratio: Signal to Noise ratio measures the variation in response with respect to the control parameters under different noise conditions.
- p-value: p-value is a quantitative measure for reporting the result of normality test. A small p-value indicates means that the null hyporhesis is false.
- T-value: T-value is the measure of ratio between the coefficient & its standard error. The magnitude of t-value decides whether to reject null hypothesis.
- SE coefficient: The standard error of coefficient measures the precision of the estimated coefficient. Smaller the standard error, more precise is the estimated value.
- AIC & BIC: These are Akaike's Information Criterion & Bayesian Information Criterion respectively. These are the measures of the relative quality of the model & this measure is dependent on number of terms in the model. Smaller values of AIC & BIC are desirable.

Table 4 (a, b) Taguchi design-orthogonal arrays & response table

(a)

Response Table for Data Means		
Level	**Speed**	**Load**
1	66.59	88.7
2	107.15	113.74
3	112.6	123.05
4	163.03	145.49
5	161.76	140.15
Delta	96.44	56.79
Rank	1	2

(b)

Response Table for S/N Ratios		
Smaller is better		
Level	**Speed**	**Load**
1	-34.38	-36.7
2	-40.1	-39.75
3	-40.95	-41.4
4	-44.07	-42.91
5	-44.01	-42.76
Delta	9.69	6.21
Rank	1	2

Tables 4(a) & 4(b) are the response tables for wear and S/N ratio of wear respectively. These S/N ratios are obtained using smaller-the-better approach. Delta is obtained by calculating the algebraic difference between the maximum & minimum

Table 5 Regression Analysis-coefficient table for wear & SN ratio of wear

Coefficients (Response is Wear)						
Term	**Coef**	**SE Coef**	**95% CI**	**T-Value**	**P-Value**	**VIF**
Constant	-90.3	30.4	(-153.4, -27.2)	-2.97	0.007	
Speed	0.1777	0.0284	(0.1189, 0.2366)	6.26	0.000	1.00
Load	0.673	0.197	(0.266, 1.081)	3.43	0.002	1.00
Coefficients (Response is SN Ratio of Wear)						
Term	**Coef**	**SE Coef**	**95% CI**	**T-Value**	**P-Value**	**VIF**
Constant	-19.88	3.52	(-27.17, -12.58)	-5.65	0.000	
Speed	-0.01676	0.00328	(-0.02356, -0.00996)	-5.11	0.000	1.00
Load	-0.0765	0.0227	(-0.1236, -0.0294)	-3.37	0.003	1.00

Table 6 Regression Analysis-model summary for wear & SN ratio of wear

Model Summary (Response is Wear)						
S	**R-sq**	**R-sq(adj)**	**PRESS**	**R-sq(pred)**	**AICc**	**BIC**
27.7901	69.85%	67.10%	21758.6	61.38%	243.99	246.86
Model Summary (Response is Signal to Noise Ratio of Wear)						
S	**R-sq**	**R-sq(adj)**	**PRESS**	**R-sq(pred)**	**AICc**	**BIC**
3.21246	62.99%	59.62%	311.304	49.25%	136.10	138.98

Table 7 Analysis of variance for wear & SN ratio of wear

Analysis of Variance (Response is Wear)							
Source	**DF**	**Seq SS**	**Contribution**	**Adj SS**	**Adj MS**	**F-Value**	**P-Value**
Regression	2	39354	69.85%	39354	19677.0	25.48	0.000
Speed	1	30289	53.76%	30289	30289.2	39.22	0.000
Load	1	9065	16.09%	9065	9064.8	11.74	0.002
Error	22	16990	30.15%	16990	772.3		
Total	24	56344	100.00%				
Analysis of Variance (Response is SN ratio of wear)							
Source	**DF**	**Seq SS**	**Contribution**	**Adj SS**	**Adj MS**	**F-Value**	**P-Value**
Regression	2	386.3	62.99%	386.3	193.17	18.72	0.000
Speed	1	269.4	43.92%	269.4	269.39	26.10	0.000
Load	1	116.9	19.07%	116.9	116.94	11.33	0.003
Error	22	227.0	37.01%	227.0	10.32		
Total	24	613.4	100.00%				

response variables. The factor with the highest delta value is assigned rank 1. Hence, the speed delta is assigned rank 1 & rank is 2 for the load delta.

$$\text{Wear} = -90.3 + 0.1777\ \text{Speed} + 0.673\ \text{Load} \quad (15)$$

$$\text{SNRA1} = -19.88 - 0.01676\ \text{Speed} - 0.0765\ \text{Load} \quad (16)$$

Eqs. (15-16) are the regression equations for wear & S/N Ratio of wear respectively. From Eqs (15-16), it is observed that the magnitude of wear as well as S/N Ratio increases with the increase in speed as well as with the increase in load.

In Table 5, T-values are obtained by dividing response coefficients (Coef) by standard error of the coefficients (SE Coef). These T-values are further used to estimate the corresponding p-values. In Table 6, the p-values for all the terms are less than the α value of 0.025 at the significance level of 5%. This indicates that both the predictor variables i.e. speed & load have a significant effect on both the response variables i.e. wear & S/N ratio. The VIF factor is 1 for both the predictors i.e. speed & load which indicates that the predictors are not correlated.

The Table 6 shows model summary for regression analysis of wear & S/N Ratio. Higher standard deviation of wear indicates lesser closeness of the observed values to the line of fit. The R^2 values for both wear and S/N Ratio are below 70 %

which indicates that the linear fit of the model can be further improved. The difference between R^2_{adj} & R^2 for both wear & S/N Ratio is below 4% and hence not much significant. It means that there are no insignificant predictors in the model. There is a substantial difference between R^2_{pred} & R^2 in case of S/N Ratio which indicates that the model is slightly over-fit. The values of AIC & BIC are a bit higher in case of both wear & S/N Ratio and if reduced would give a better linear fit.

Table 7 shows a result of Analysis of Variance (ANOVA) for wear and S/N Ratio. Higher values of sequential sum of squares & percentage contribution for speed as compared to load indicates that the speed factor accounts for more deviance in the response variable wear as well as in S/N Ratio. From Table 7 it is seen that both the speed & load factors have significant effects on the response variable wear as well as on S/N Ratio.

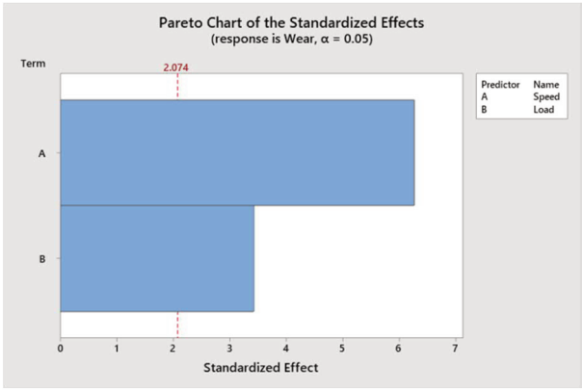

(a)

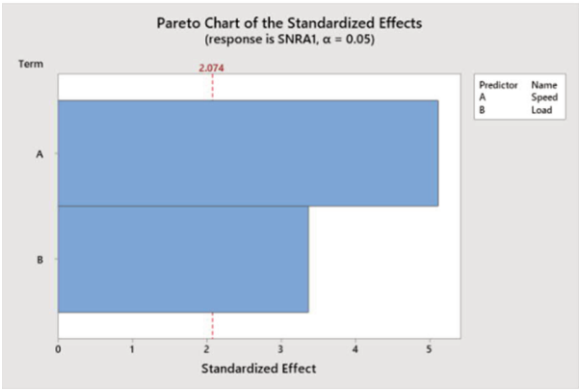

(b)

Fig. 11 Pareto charts of standardized effects (a) Response is wear (b) Response is S/N Ratio

Fig.11 shows Pareto charts in which the absolute values of standardized effects for the predictors A (speed) and B (Load) are plotted. In Fig.11(a), wear is the response variable. In Fig.11(b), signal-to-noise ratio is the response variable. The bars which cross the reference line are statistically significant. In Fig.11 both the bars cross the reference line which indicates that both the factors speed and load have a significant effect on the response variables wear as well as on signal-to-noise ratio of wear.

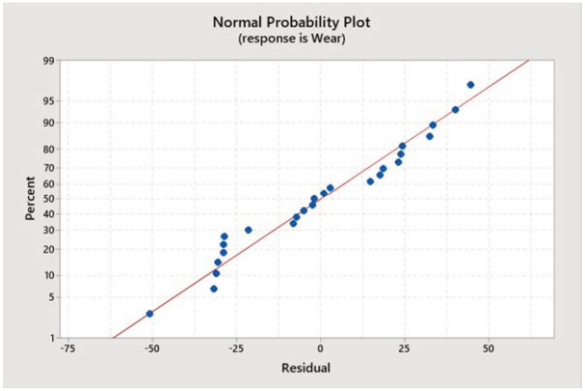

(a)

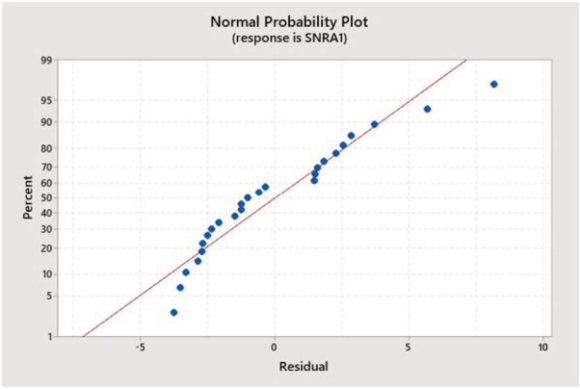

(b)

Fig. 12 Half-Normal probability plots (a) Response is wear (b) Response is S/N Ratio

Fig.12(a-b), shows the percentage cumulative normal probability of the effects with the residual values. In Fig.12(a), 13 out of 25 residuals fall on or very close to the line of fit. The remaining 12 residuals which fall away from the line of fit are said to have a significant effect on the response. In Fig.12(b), 9 out of 25 residuals fall on or very close to the line of fit. The remaining 16 residuals which fall away from the line of fit are said to have a significant effect on the response.

The Fig. 13 shows the variation of residual versus the fitted values when (a) the response variable wear and (b) response is S/N Ratio. From Fig. 13 it is observed that the scattering of data follows different patterns in different ranges of fitted value. This pattern is known as heteroscedasticity. It means that the distribution of residuals is uneven in different ranges of fitted values of the response.

In Fig.13(a), in the range (0 to 75), the residuals lie in the negative region. In the range (75 to 125), the residuals are uniformly scattered about the zero line & are close to the zero line. In the range (125 to 175), the residuals are uniformly scattered about the zero line & are away from the zero line. In the range (175 to 200), the residuals are very close to the zero line.

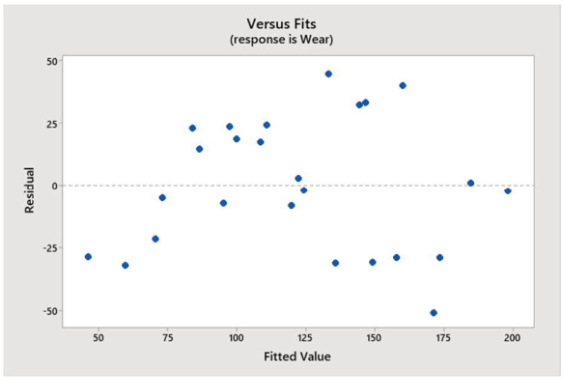

(a)

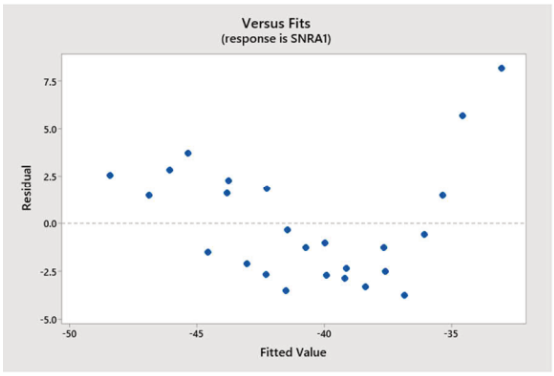

(b)

Fig. 13 Residual versus fitted values (a) Response is wear (b) Response is S/N Ratio

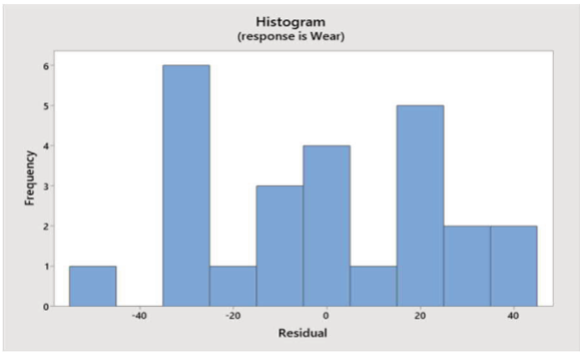

(a)

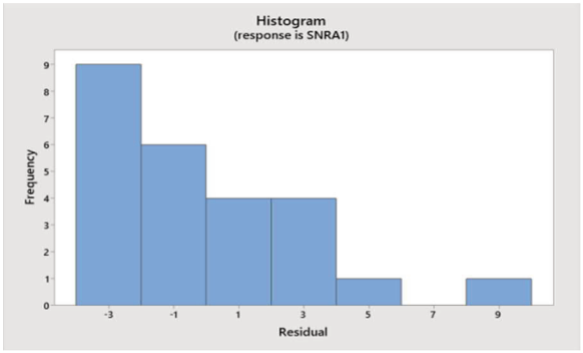

(b)

Fig. 14 Histogram of residual versus frequency (a) Response is wear (b) Response is S/N Ratio

In Fig. 13 (b), in the range (-50 to -45), the residuals are uniformly scattered about the zero line and are close to the zero line. In the range (-45 to -40), the residuals are scattered more in the negative region. Some residuals are close to the zero line & some are away from the line. In the fitted value range (-40 to -35), the residuals are scattered densely in the negative region. Some residuals in this region are positive in nature & are located away from the zero line.

Figs.14(a-b) show histograms of residuals. In Fig.14(a), the frequency of residuals is higher in the residual ranges (-25 to -35) and (15 to 25) than the frequency at the center. Hence, the histogram deviates from the bell-shaped normal distribution curve. In Fig.14(b), the frequency of residuals is higher in the range of residuals (-2 to -4) than the frequency at the center. Hence, this histogram also deviates from the bell-shaped normal distribution curve.

Figs.15(a-b) are the interaction plots for data means of the response variables wear & S/N ratio respectively. Load & speed are the predictor variables. These interaction plots show how a response variable varies when one predictor variable is kept constant & the other is varied. In Fig.15(a), the top right plot shows variation in wear with load for five different levels of speed & load. The bottom left plot shows variation in wear with speed for five different levels of load & speed. Similarly in Fig.15(b), the top right plot shows variation in S/N ratio with load for five different levels of speed and load. The bottom left plots show variation in S/N ratio with speed for five different levels of load and speed.

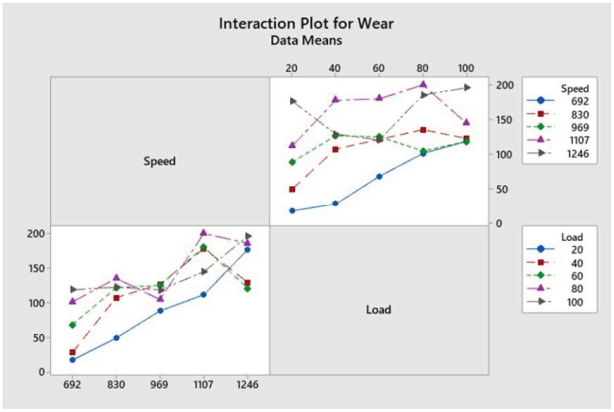

(a)

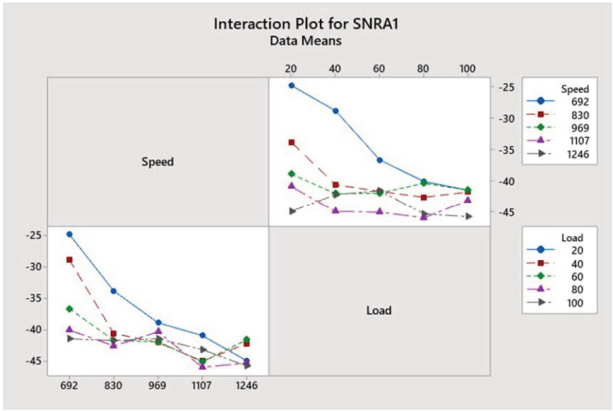

(b)

Fig. 15 Interaction Plots for (a) response is wear (b) response is S/N Ratio

6. CONCLUSIONS

- In this work, experimental analysis of rolling & sliding contact between the outer surface of the inner race of a cylindrical roller bearing & the outer surface of the cylindrical roller is carried out using pin-on-disk apparatus. The objective of this research work is to estimate the wear (μm) of the EN31 alloy steel roller followed by statistical analysis using the commercial package MINITAB-19 to plot the line of best fit.
- During pin-on-disk experimentation, maximum magnitude of wear was found to be 200.33 μm at 80 N load and 1107 RPM speed condition. The minimum value of wear was found to be 17.41 μm at 20 N load & 692 RPM speed condition. The regression coefficient for load in the equation for wear obtained from MINITAB is 0.673, whereas the coefficient for speed is 0.178. Hence, it is concluded that the load factor has more effect on wear than the speed factor and wear increases with the increase in load as well as with the increase in speed.
- From the regression model summary, it is observed that R^2_{adj} differs from R^2 by less than 4%. Hence, it is concluded that there is no significant effect of unnecessary terms on the regression model. The maximum difference between R^2_{pred} and R^2 is 13.7 %. Hence, it is concluded that the model is slightly over-fit & it can be improved.
- From the experimental and statistical analyses, it is concluded that there is a further scope for research in order to improve the model. The results can be improved by conducting extensive experimentation for the unsatisfactory results i.e., the residuals which fall away from the line of fit. Experimentation & statistical analysis can be performed again until the results are satisfactory in terms of quality of the model.

Financial and Ethical disclosures: This work is not supported fully or partially by any funding organization or agency.

Conflict of interest: The authors declare that there is no conflict of interests regarding the publication of this paper.

List of Symbols

c_{coeff}	Coefficient based on Shape, Processing Accuracy & Material
c_{rf}	Rating Factor based on Material & Manufacturing Quality
C_{Dyn}	Dynamic Load carrying Capacity of the Bearing (N)
C_{st}	Static Load carrying Capacity of the Bearing (N)
D_d	Disk Dia. of the Pin-on-Disk Machine (mm)
D_o	Outside Dia. of the Outer Race (mm)
D_{pr}	Pitch Circle Dia. of the Bearing (mm)
D_r	Outside Dia. of the Roller (mm)
D_{s0}	Outside Dia. of the Shaft (mm)
D_t	Track Dia. of the Disk (mm)
L_{10}	Bearing Life (million revolutions)
L_{10h}	Bearing Life (hours)
L_{eff}	Effective Length of the Roller (mm)
L_b	Width of the Bearing (mm)
L_r	Length of the Roller (mm)
n_{roller}	Number of Rollers per Row
n_{row}	Number of Rows of Rollers in each Bearing
N_d	Disk Rotational Speed (RPM)
N_i	Inner Race Rotational Speed (RPM)
N_o	Outer Race Rotational Speed (RPM)
N_r	Roller Rotational Speed about the Shaft Axis (RPM)
N_R	Roller Rotational speed about its own axis (RPM)
P	Radial Load acting on each Cylindrical Roller (N)
P_T	Radial Load acting on the Bearing (N)
V_r	Roller Centerline Linear Speed (mm/s)
V_{ri}	Roller Linear Speed relative to the Inner Race (mm/s)
V_{ro}	Roller Linear Speed relative to the Outer Race (mm/s)
β	Angle between two adjacent Cylindrical Rollers (Degree)
γ	Nominal Contact Angle (Degree)

7. REFERENCES

1. Harris T. & Kotzalas M., Essential Concepts of Bearing Technology, CRC Press-Taylor & Francis Group, Fifth Edition (2007). https://doi.org/10.1201/9781420006582
2. Beswick J., Bearing Steel Technology. American Society for Testing & Materials Int. (ASTM Press), ASTM Stock Number STP 1419 (2002).
3. Bhushan B., Introduction to Tribology, John Wiley & Sons Ltd., 2nd Edition (2013). https://doi.org/10.1002/9781118403259
4. Bhandari V. B., Design of Machine Elements, The McGraw-Hill Companies, 3rd Edition (2007).

5. Guillermo E., Wallin H., Hauleitner R. & Arvidsson M., Progress in Rolling Bearing Technology for Refrigerant Compressors, Proceedings of the Institution of Mechanical Engineers Part C: Journal of Mechanical Engineering Science, SAGE, ISSN: 0954-4062 (2017).

6. Li F., Hu W., Meng Q., Zhan Z. & Shen F., A New Damage-Mechanics-based Model for Rolling Contact Fatigue Analysis of Cylindrical Roller Bearing, Tribology International (Elsevier), S0301-679X(17) 30560-1, JTRI 4985 (2017).

7. Liu Y., Zhu Y., Yan K., Wang F., Hong J., A Novel Method to Model effects of Natural Defect on Roller Bearing., Tribology International (Elsevier), Vol. 122, PP. 169-178 (2018). https://doi.org/10.1016/j.triboint.2018.02.028

8. Panda S., Panda S.N., Nanda P. & Mishra D., Comparative Study on Optimum Design of Rolling Element Bearing, S0301-679X (15) 00325-4, JTRI3769 (2015).

9. Feldermann A., Fischer D., Neumann S. & Jacobs G., Determination of Hydraulic Losses in Radial Cylindrical Roller Bearing using CFD Simulations, Tribology International (Elsevier), S0301-679X (17) 30137-8, JTRI4648 (2017).

10. Denni M., Biboulet N., Abousleiman V. & Lubrecht A., Dynamic Study of a Roller Bearing in a Planetary Application considering the Hydrodynamic Lubrication of the Roller/Cage Contact, Tribology International, 0301-679X (2019) https://doi.org/10.1016/j.triboint.2019.03.054

11. Laithy M., Wang L., Harvey T., Vierneusel B., Correns M. & Blass T., Further understanding of Rolling Contact Fatigue in Rolling Element Bearings, Tribology International (Elsevier), Vol. 140 Art. 105849 (2019). https://doi.org/10.1016/j.triboint.2019.105849

12. Zhang H., Wang W., Zhang S. & Zhao Z., Modeling of Elastic Finite-Length Space Rolling-Sliding Contact Problem, Tribology International (Elsevier), 0301-679X (2016). https://doi.org/10.1016/j.triboint.2016.10.045

13. Guo Y. & Keller J., Validation of Combined Analytical Methods to predict Slip in Cylindrical Roller Bearings, Tribology International (Elsevier), Vol. 148 PP. 106347 (2020). https://doi.org/10.1016/j.triboint.2020.106347

14. Ahmer S., Jan L., Siddig M. & Abdullah S., Experimental Results of the Tribology of Aluminium Measured with a Pin-on-Disk Tribometer: Testing Configuration & Additive Effects, Friction: 4(2): 124-134 (2016). https://doi.org/10.1007/s40544-016-0109-7

15. Stratmann A., Jacobs G., Hsu C. , Gachot C. & Burghardt G., Antiwear Tribofilm Growth in Rolling Bearings under Boundary Lubrication Conditions, Tribology International (Elsevier), 0301-679X (2017). https://doi.org/10.1016/j.triboint.2017.03.030

16. El-Thalji I. & Jantunen E., Dynamic Modelling of Wear Evolution in Roller Bearings, Tribology International (Elsevier), Vol. 84 PP. 90-99 (2015). https://doi.org/10.1016/j.triboint.2014.11.021

17. Takabi J. & Khonsari M., On the Dynamic Performance of Roller Bearings operating under Low Rotational Speeds with consideration of Surface Roughness, Tribology International (Elsevier), Vol.86 PP. 62-71 (2015). https://doi.org/10.1016/j.triboint.2015.01.011

18. Eyre T., Wear Characteristics of Metals, Tribology International (Elsevier), ISSUE: OCT, PP 203-212 (1976). https://doi.org/10.1016/0301-679X(76)90077-3

19. Zhang X., Kanapathipillai S., Wu T. & Peng Z., Frictional Behavior & Friction Mechanisms of Rolling-Sliding Contact in Mixed EHL, Tribology International (Elsevier), Vol. 114 PP. 201-207 (2017). https://doi.org/10.1016/j.triboint.2017.04.032

20. Gawande S. & Patil A., Experimental Study on Tribological Characteristics of Steel Alloys for CNC Bending Machine, Journal of Bio-and Tribo-Corrosion (2018) 4:72. https://doi.org/10.1007/s40735-018-0191-7

21. Dhanvij N., Gawande S.H. & Gajjal P., Performance Evaluation of EN24 for Planetary Gear Transmission of CNC Bending Machine, Journal of the Brazilian Society of Mechanical Sciences & Engineering (Springer), Vol. 42, Issue 298 (2020). https://doi.org/10.1007/s40430-020-02392-5

22. Nicholas G., Howard T., Long H., Wheals J. & Dwyer-Joyce R., Measurement of Roller Load , Load Variation & Lubrication in a Wind Turbine Gearbox High Speed Shaft Bearing in the Field, Tribology International (Elsevier), Vol. 148 ISS. 106322 (2020). https://doi.org/10.1016/j.triboint.2020.106322

23. Cavacece F., Frache L., Tonazzi D., Bouscharain N., Philippon D., Le Jeune G., Maheo Y. & Massi F., Roller Bearing under High Loaded Oscillations: Life Evolution & Accomodation Mechanisms, Tribology International (Elsevier), Vol. 147 : Issue 106278 (2020). https://doi.org/10.1016/j.triboint.2020.106278

24. Paulson N., Golmohammadi Z., Walvekar A., Sadeghi F. & Mistry K., Rolling Contact Fatigue in Refurbished Case Carburized Bearings, Tribology International (Elsevier), Vol. 115: Issue 348-364 (2017). https://doi.org/10.1016/j.triboint.2017.05.026

25. Salguero J., Martinez J., Sol I. & Batista M., Application of Pin-on-Disc Techniques for the Study of Tribological Interferences in the Dry Machining of A92024-T3 (Al-Cu) Alloys, Materials (MDPI) 11:1236 (2018). https://doi.org/10.3390/ma11071236

26. Krishnaiah K. & Shahabudeen P., Applied Design of Experiments & Taguchi Methods, PHI Learning Pvt. Ltd. (2012).

27. Mathews P., Design of Experiments with MINITAB, ASQ Quality Press (2005).

28. Taguchi G., Chowdhury S. & Wu Y., Taguchi's Quality Engineering Handbook, John Wiley & Sons Inc. (2005). https://doi.org/10.1002/9780470258354